Rheologica Acta (2025) 64:241–253
https://doi.org/10.1007/s00397-025-01499-7

ORIGINAL CONTRIBUTION

Microrheological characterisation of clay-PEO nanocomposites

Iliya D. Stoev[1] · Anasua Mukhopadhyay[2] · Rene Tammen[3] · Erika Eiser[3]

Received: 25 February 2025 / Revised: 2 May 2025 / Accepted: 15 May 2025 / Published online: 6 June 2025

Abstract
Clay-polymer mixtures, characterised by high mechanical stiffness, are widely utilised in strengthening soft and easy-to-break materials. Here, we present microrheological results on shake-gels made of natural (montmorillonite) and synthetic (Laponite) disk-shaped clay particles in combination with poly(ethyleneoxide). These clay-polymer suspensions represent shear-thickening fluids that display a large increase in viscosity upon large-amplitude shaking. By performing both bulk and microrheology experiments, we probe the phase behaviour and mechanical response of these nanocomposites. Slight tuning of either the particle or polymer concentration leads to dramatic changes in the macroscopic appearance of the mixture, transitioning from a low-viscosity fluid to a stiff gel, capable of sustaining its own weight. We relate these observations to microscopic measurements, providing insight into the local reorganisation of the constituting building blocks and the time-evolution of each phase.

Keywords Microrheology · Light scattering · Shake gels · Laponite · Montmorillonite

Introduction

Clays are naturally occurring layered mineral materials that have garnered significant interest over recent decades due to their versatile industrial applications in paint production, drilling fluids, personal care product design, cosmetics, coatings and pharmaceutical formulations (Murray 2000). Recent advancements have highlighted the unique properties of Laponite (Lap) and montmorillonite (MMT) as clay particles of particular interest for developing functional materials. These clays are selected due to their high specific areas and exceptional polymer-binding capabilities, which allow for the creation of materials with tunable mechanical properties (Raji et al. 2016; Jin et al. 2002; Brostow et al. 2010; Tyan et al. 2001).

The aim of this investigation is to explore the specific interactions between these two types of clays and polyethylene oxide (PEO), a common polymer, and how these interactions influence their rheological properties. Such insights could further enhance their application scope in targeted industries.

MMT, naturally occurring and a key component of bentonite (van Olphen 1977), represents an expanding 2:1 layered clay with a chemical structure of $Na_{0.33}[(Al_{1.67}Mg_{0.33})Si_4O_{10}(OH)_2]\bullet nH_2O$. Upon exfoliation, MMT disperses into platelets approximately 1-nm thick with diameters ranging from 50 to 500 nm (Leach et al. 2005; Ho et al. 2001).

Conversely, Laponite is a synthetic hectorite distinguished by its smaller size, with platelets approximately 1-nm thick and 30 nm in diameter. Its chemical structure is represented as $Na_{0.7}([Si_8Mg_{5.5}Li_{0.3}O_{20}(OH)_4])$ (Bonn et al. 1999a, b). In aqueous colloidal suspensions, Laponite can readily form either a gel or a Wigner glass at relatively low concentrations (Ramsay 1986; Mourchid et al. 1995; Pignon et al. 1997; Lemaire et al. 2002).

Even though the basic structure of Laponite and MMT is similar, the different substitutions alter their individual interactions with polymers. The underlying mechanism of physisorption depends on the surface charge of the clay

✉ Iliya D. Stoev
iliya.stoev@kit.edu

✉ Erika Eiser
erika.eiser@ntnu.no

[1] Institute of Biological and Chemical Systems – Biological Information Processing, Karlsruhe Institute of Technology, Karlsruhe 76344, Germany

[2] Adolphe Merkle Institute, University of Fribourg, Fribourg 1700, Switzerland

[3] PoreLab, Department of Physics, Norwegian University of Science and Technology, Trondheim N-7491, Norway

particles, which is in turn linked to the association of solvent counterions.

The unique electrostatic characteristics of these clays—featuring negatively charged surfaces and pH-dependent positively charged rims—facilitate their self-assembly into higher-order structures (van Olphen 1977). These interactions, along with the aging process into a disordered, amorphous phase, can be intricately influenced by manipulating the ionic strength and temperature of the solution (Ramsay 1986; Li et al. 2005). Here, we specifically focus on comparing the gelation behaviour of Lap and MMT when mixed with PEO, thereby elucidating the fundamental mechanisms behind their differing rheological outcomes and understanding why these clays, in particular, form shake-gels effectively.

PEO is a non-ionic polymer, which upon addition to clay aqueous suspensions modifies their rheological properties due to the adsorption of polymer chains on the surface of the clay particles, thus altering their phase behaviour (Morariu and Bercea 2009; Xu et al. 2018). Mixtures of Lap and PEO have been studied extensively in the literature, exploring the effect of pH and ionic strength, molecular weight of PEO as well as Lap concentration (Baghdadi et al. 2005; Baghdadi et al. 2008a, b; Bonn et al. 1999b; Bonn et al. 2002a, b; Levitz et al. 2000; Mourchid and Levitz 1998; Mourchid et al. 1995, 1998; Schmidt et al. 2000, 2002; Zebrowski et al. 2003). Zebrowski et al. 2003 reported a shear-induced transition from a low-viscosity fluid (cf. later type 1) into a 'shake-gel' (cf. later types 2 and 3) for certain concentrations of Lap and PEO. They have outlined the mechanism of shake-gel formation with the help of both static and dynamic light scattering measurements. At first, shaking causes PEO to weakly adsorb onto the surface of the Lap particles, facilitating the formation of finite-size aggregates. Application of strong shear can lead to polymer desorption and loss of contact points between the PEO and the clay, following re-adsorption of PEO onto the particle surface. Thus, individual clay disks or clusters are bridged into a percolating gel network. During relaxation, the desorption of the polymer chains reduces the degree of bridging, which reduces the stiffness of the gel network.

Here, we employ rheology studies to understand the macroscopic behaviour and gelation mechanisms of these nanocomposites. Lap-PEO mixtures have been primarily studied through bulk rheology measurements. Baghdadi et al. (2008a, b) demonstrate the importance of the clay-polymer ratio in the case of using Lap and PEO. At low PEO concentrations, the overall phase behaviour is dominated by clay aging, whereas at high PEO concentrations there is a switch-over in the contributions of the clay and polymer marked by a shift in the relative dominance of the elastic and viscous moduli (Baghdadi et al. 2008a, b).

The sub-millisecond absorption–desorption in these systems calls for the use of microrheology, where the MHz acquisition speed of an autocorrelator enables extracting the high-frequency response. Autocorrelation functions characterising the diffusion of probe particles are converted into mean-squared displacement (MSD). The latter is then transformed into the material's viscoelastic modulus G(s) according to the Generalised Stokes–Einstein Relation (GSER):

$$G(s) = \frac{k_B T}{\pi a s \bigtriangleup \tilde{r}^2(s)} \tag{1}$$

with thermal energy as $k_B T$, the bead radius as a, and the unilateral Laplace transform of the MSD as $\bigtriangleup \tilde{r}^2(s)$ (Mason 2000).

Here, we combine conventional bulk rheology with microrheology to probe the dynamic viscoelastic behaviour of differently concentrated Lap-PEO and MMT-PEO mixtures. Shake-gels of high turbidity are analysed via diffusing wave spectroscopy, where the technique benefits from the complete randomisation of the photon path. Through leveraging the different optimal ranges of operation of each technique, we present a comprehensive picture of the macro- and microscopic mechanics of Lap-PEO and MMT-PEO clay-polymer nanocomposites.

Experimental

Clay-PEO nanocomposite preparation

Lap XLG and MMT, both acquired from Rockwood Additives Ltd., were first dispersed in deionised water (purified by a Milli-Q Academic System, Millipore Cooperation) at a stock concentration of 2.0%w. The samples were then stirred for 24 h at 500 rpm using magnetic stir bars for complete exfoliation. Similarly, 2%w poly(ethyleneoxide) (400 kDa PEO, Sigma-Aldrich) was dissolved in deionised water. After completing the clay exfoliation and fully dissolving the polymer, we used the stock batches to prepare mixtures of Lap-PEO and MMT-PEO solutions. In constructing the phase diagrams, the reported concentrations of clay and polymer were mixed together and vigorously shaken manually with repeated back-and-forth motion that effectively applied a combination of shear and extensional stresses to the samples. We note that shearing the samples controllably in a bulk rheometer did not lead to the formation of shake-gels, which may partially rely on the entrapment of air, leading to increased turbidity and viscosity. The different phases obtained as a result of this vigorous shaking were split into categories (types 1–3 for Lap-PEO and types I–III for MMT-PEO complexes), visualised in Fig. 1 and documented in Table 1. In the following mechanical

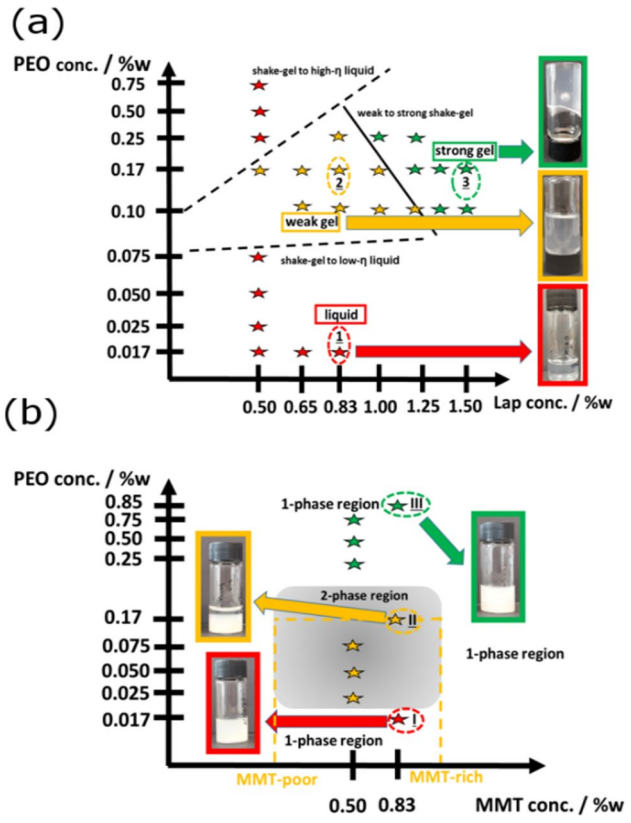

Fig. 1 Schematic phase diagrams based on qualitative observations of freshly prepared and shaken **a** Lap-PEO and **b** MMT-PEO mixtures, showing the three types of suspensions investigated in this work (red, yellow and green stars). In the case of Lap, we distinguished between a liquid (type 1), a weak gel (type 2) and a strong gel (type 3), whereas using MMT we obtained either low-viscosity homogeneous fluid (type I), phase-segregated sample (type II) or high-viscosity homogeneous mixture (type III)

the preparation required either gentle mixing or vigorous shaking, as specified individually for each measurement.

Bulk rheology (BR)

We used a stress-controlled bulk rheometer (Physica MCR 501, Anton-Paar) equipped with either a Couette concentric cylinder geometry (CC27, 27-mm base diameter, stainless steel) for oscillatory shear, or cone-and-plate geometry (CP25-2/TG, 25-mm base diameter, 2° cone angle) for creep measurements. Frequency ramps were obtained through oscillatory shear measurements, performed at 1% strain amplitude. Creep step-stress (10 min on, 10 min off) measurements were performed by progressively increasing the stress and following the creep behaviour of the test mixture at each applied stress. Oscillatory shear and creep measurements were performed at 25 °C. Custom-made 3D-printed vapour trap was used to minimise evaporation from the sample throughout these measurements.

Dynamic light scattering (DLS)

Malvern Zetasizer ZSP (633 nm HeNe laser) equipped with temperature control was used for performing microrheology on Lap-PEO and MMT-PEO mixtures. The probe-particles were 230-nm PS-PEG (poly(ethyleneglycol)-coated polystyrene latex) obtained from Cambridge Bespoke Colloids, UK. To ensure the detection of single-scattering events, we operated our setup at 173°, non-invasive backscatter (NIBS) detection mode. The probe concentration was 0.03%w in all measurements, ensuring dominant scattering (ca. 95%) from the probe-particles. Measurements were conducted in

Table 1 Appearance and classification of various clay nanocomposites according to their viscosity (η) and concentration of Lap/MMT and PEO (also shown schematically in Fig. 1)

Type	Lap Conc. / %w	PEO Conc. / %w	Appearance
1 ★	0.50-1.00	0.017-0.075	liquid
2 ★	0.50-1.00	0.075-0.250	weak gel
3 ★	1.25-1.50	0.075-0.250	strong gel
Type	**MMT Conc. / %w**	**PEO Conc. / %w**	**Appearance**
I ★	0.25-1.00	0.010-0.020	low-η liquid
II ★	0.25-1.00	0.020-0.200	two phases
III ★	0.25-1.00	0.200-1.000	high-η liquid

tests, samples belonging to each group were selected, where

disposable cuvettes (40 µL, ZEN0040, Malvern). The attenuator and detector measurement positions were automatically optimised to achieve high signal-to-noise acquisition. All measurements were performed at 25 °C.

In the conversion of intensity autocorrelation functions $g^{(2)}$ (t) into intermediate scattering functions $g^{(1)}$ (t), we employed the Siegert relation:

$$g^{(2)}(t) = 1 + \beta\left|g^{(1)}(t)\right|^2, \tag{2}$$

where β represents the zero-time intercept of $g^{(2)}$ (t) –1, and $g^{(1)}$ (t) was fitted to a multi-exponential decay function through CONTIN (constrained regularisation method) (Provencher 1982) via an in-house Matlab routine. Fitting the measured experimental curves allowed high-quality, artifact-free conversion from real to Fourier space (Maier et al. 2012). The MSD of the probe-particles, used in obtaining the complex viscoelastic modulus via Eq. (1), was first estimated through the following relation:

$$g^{(1)}(t) = e^{-q^2 \triangle r^2(t)/6,} \tag{3}$$

where q was the scattering wavevector.

Diffusing wave spectroscopy (DWS)

DWS spectrometer (RheoLab, LS Instruments) equipped with a temperature controller and operated in transmission mode was calibrated using 1%w polystyrene colloids (200-nm radius, LS Instruments) stabilised by sulphate groups in water. The transport mean free path in the sample, relative to a reference scattering length, was estimated by the software using the relation:

$$l^*(sample) \approx \left(\frac{CR_{sample}}{CR_{ref}}\right) l^*(ref), \tag{4}$$

where CR is the measured photon count rate (ca. 300 kHz for both sample and reference). We ran the calibration and subsequent tests at 25 °C. The sample cuvette had a thickness of 1 mm and was sealed with parafilm to prevent evaporation. At the start of each measurement, we set the multiple-tau correlation time to 270 s and the echo duration to 150 s.

The intensity autocorrelation function outputted by the digital correlator is given by:

$$g^{(2)}(t) - 1 = I(t)I(0)/I^2, \tag{5}$$

which was subsequently fitted using the 'two-cell' technique (Harden and Viasnoff 2001). Utilising the fluctuation–dissipation relation for the conversion into MSD (Weitz et al. 1993), the complex viscoelastic modulus was then calculated via the GSER (Mason and Weitz 1995). The generality of the autocorrelation fit prior to the conversion into viscoelastic modulus removed the need for pre-fitting to any particular theoretical model, thus ensuring the unbiased analysis of microrheological data.

Optical trapping (OT)

We used a custom-made optical-tweezer system based on a Thorlabs model OTKB/M, equipped with a laser diode of 975-nm wavelength (cf. Stoev et al. 2018 for details). The tracer particles were 1.5-µm SiO_2 colloids (Microparticles GmbH, Germany) diluted 10,000 times and surface-coated with poly(L-lysine)-poly(ethyleneglycol) with grafting ratio of PLL(20 kDa)-g(3.5)-PEG(2 kDa). Broadband viscoelasticity of the test sample was extracted through stitching long and short acquisitions with sampling rates of 10 kHz and 1 MHz, respectively. The trajectory of the tracer bead was recorded using an InGaAs quadrant photodiode and then converted into a position autocorrelation function and viscoelastic modulus via in-house Matlab routines, following the analysis of Evans et al. 2009.

Results and discussion

Types of Laponite-PEO nanocomposites

Zebrowski et al. (2003) first reported the shear-induced gelation of Lap-PEO mixtures at moderate polymer concentrations, which we confirmed in a schematic phase diagram (denoted as type 2 samples in Fig. 1a). At first these samples appeared turbid due to local aggregation, but then relaxed when left unperturbed, where the relaxation time was strongly dependent on the clay concentration. Cabane et al. (1997) first explained the formation of these shake-gels as facilitated by silica-PEO complexation. The proposed mechanism involved the repeated adsorption and desorption of PEO chains onto the exposed silica on the clay surface. The higher number of polymer–clay contacts was associated with more effective polymer bridging between the disk-shaped colloids. However, this microscopic behaviour only manifests on the macroscale as a gel provided that there are sufficient clay particles (cross-link points) and polymer chains to enable aggregation.

In addition, Can and Okay 2005 reported a notable distinction between shake-gels formed at low and high Lap concentrations, in agreement with the phase diagram in Fig. 1a. Using 400 kDa PEO, we found an abrupt transition from a weak, lumpy, stress-compliant shake-gel (type 2) to a strong, percolating shake-gel, capable of sustaining its own weight (type 3). We identified the slanted boundary as the percolation threshold, where higher clay concentration required lower amount of polymer to form a volume-spanning aggregate.

Depending on the final polymer and clay concentrations, the outcomes observed on shaking Lap-PEO solutions followed three main categories (Table 1). Preparing a mixture of low concentrations of clay and PEO resulted in a transparent liquid (type 1) that maintained its appearance even after mechanical agitation. Here we noted two main observations: first, mixtures that had insufficient polymer were unable to form macroscopic aggregates, with the bridging leading only to finite-size clusters comprised of only a few particles; moreover, although pure Lap suspensions are known to age (Ruzicka and Zaccarelli 2011), at the reported low clay concentrations the transition into a gel would require months of waiting time. As all samples were prepared and used fresh, any gelation that we observed was accredited to the presence of the polymer.

On increasing the polymer concentration, such that the mole ratio between PEO and Lap is greater than one, we achieved full coverage of the clay disks, resulting again in a type 1 fluid. The particles, in this case, were sterically stabilised, and the overall dynamics were dominated by the excess polymer, contributing to the increase in the bulk viscosity of the entire mixture.

Types of MMT-PEO nanocomposites

To facilitate the direct comparison with Lap-PEO mixtures, we studied similar compositions of MMT-PEO (Fig. 1b), where we encountered a notably different phase diagram. At low MMT and PEO concentrations, the mixtures remained liquid (type I), similar to Lap-based suspensions. As before, we attributed the fluidity to the absence of sufficient polymer to associate the particles into macroscopic clusters. MMT suspensions on their own tend to phase separate into a disordered anisotropic clay-rich phase and a completely isotropic clay-poor liquid (Langmuir 1938). Akin to the aging in Lap suspensions, this process of phase separation requires waiting time on the order of weeks or even months, depending on the clay concentration. Here, we observed accelerated macroscopic phase separation within a few hours on shaking freshly prepared intermediate concentrations of PEO and MMT (shake-gels denoted as type II mixtures in Fig. 1b). We used refractive index measurements (data not shown) on the MMT-poor supernatant in our phase-separated samples to confirm that most of the PEO and clay were consumed in forming the MMT-rich phase. This implied that the process of phase separation was unlikely to be driven by osmotic pressure differences, which would instead cause particle influx towards the clay-poor phase. Instead, we reconciled these observations with two facts: first, the pure MMT phase separates due to its large size and lower degree of exfoliation in water; second, polymer bridging creates larger clay clusters, thereby accelerating the sedimentation process. Fourier-transform infrared (FTIR) spectroscopy (cf. Supplementary Information) confirmed the polymer adsorption onto the MMT surface. Finally, increasing the concentration of MMT up to ca. 1.5%w (data not shown) at a fixed PEO concentration of 0.17%w led to a percolating shake-gel without phase separation after months.

Increasing the PEO concentration to $\gtrsim 0.20$%w at concentration of MMT 0.25–1.00%w resulted again in a liquid sample (type III fluid), which was more viscous than the samples formed at lower PEO concentrations. This re-entrant behaviour was reminiscent of the shake-gel formation in Lap-PEO suspensions, following a similar interpretation. One distinction between liquid samples containing low and high PEO concentrations was the appearance of foam in the latter when shaken due to the presence of excess surface-active polymer.

As shown in Fig. 1b, the MMT-PEO mixtures appeared yellow in colour as in pure MMT aqueous dispersions. Since MMT is a natural clay, one could attribute this to a wide particle size distribution, possibly containing metal impurities. Assuming an average platelet radius of 100 nm following exfoliation, the gravimetric height ($h \backsim k_B T/(mg,)$ with particle mass m and gravitational acceleration g) is around 1 mm; hence, the long time required for sedimentation of pure MMT suspensions. On adding PEO, the polymer-mediated particle aggregates were of much larger size, comprising hundreds or even thousands of MMT disks. As a consequence, the gravimetric height was much smaller leading to an accelerated sedimentation.

In the following rheological analysis, we provided further insight into the mechanism of formation and final structure of these shake-gels immediately following a mechanical agitation. We merged conventional bulk rheology with passive microrheology to leverage the capabilities of each technique in providing viscoelastic information on different timescales.

Bulk rheology on Lap-PEO NCs

We performed both oscillatory shear (Fig. 2a) and creep (Fig. 3a) measurements on a weak shake-gel (type 2) consisting of 0.83%w Lap and 0.17%w PEO. The frequency ramps showed the dominance of the storage modulus $G'(\omega)$ over the loss modulus $G''(\omega)$. This confirmed the gelation of the sample upon shaking, with a characteristic difference of one order of magnitude between the two moduli. Attempts to load fresh unperturbed sample into the shear rheometer and apply high shear rates to controllably mimic the shaking process did not result in the formation of a shake-gel. This emphasises the importance of combining shear with extensional stresses to stretch the polymer, which is sufficiently long ($\approx$ 34 nm radius of gyration for 400 kDa PEO) to bridge clay particles together. This bridging we expect to occur when the distance between exposed silica surfaces is approximately 2–2.5 times the radius of gyration of the 400 kDa PEO. According

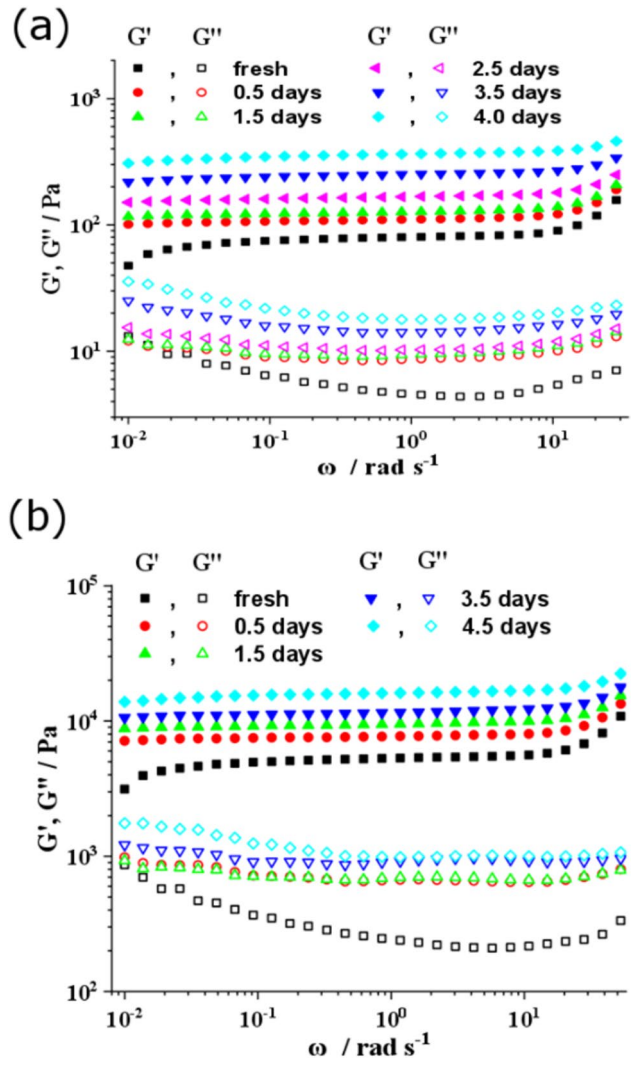

Fig. 2 Frequency ramps showing the time-evolution of the storage (G′(ω), filled symbols) and loss (G″(ω), empty symbols) moduli of **a** weak shake-gel of composition 0.83%w Lap and 0.17%w PEO (sample 2 in Fig. 1a) and **b** strong shake-gel of composition 1.50%w Lap and 0.17%w PEO (sample 3 in Fig. 1a). These oscillatory measurements were performed at a fixed oscillatory strain of 1%

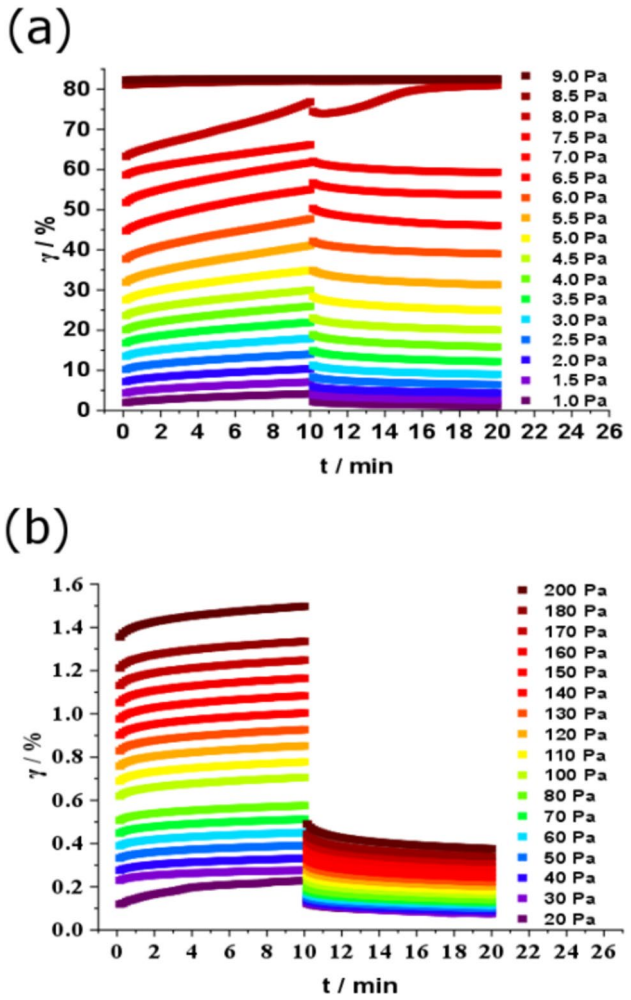

Fig. 3 **a** Step-stress measurements on a fresh sample of 0.83%w Lap and 0.17%w PEO (the type 2 shake-gel from Fig. 2a); the changes in strain for stresses lower than 8.0 Pa reflect the creep behaviour of the relaxing material. At higher stresses, the sample ruptured (deformed plastically). **b** Step-stress measurements on a fresh sample of 1.50%w Lap and 0.17%w PEO (the type 3 shake-gel from Fig. 2b). The sample deformed only by ca. 1% at 150 Pa, showing significant enhancement in mechanical strength compared to the sample in **a**

to Zebrowski et al. (2003), PEO adsorbs onto Laponite reversibly via physisorption, with an energy about 1.2 k_BT. On removing the external stress, one would expect thermal fluctuations to relax the gel, lowering its moduli. In Fig. 2, we observed stiffening of the gel instead, which we speculate to be due to electrostatically driven aggregation of uncoated Lap into clusters. This suggestion would be supported by the concentration imbalance between clay and PEO, where the excess Lap freely diffused and attached to already formed clusters, thus further strengthening the gel. This accrual process may have continued until all the clay from the bulk was consumed in forming the gel.

To enable direct comparison between the two types of shake-gels, in Fig. 2b, we tracked the viscoelasticity of a strong shake-gel (type 3) containing the same PEO concentration of 0.17%w, but nearly twice the Lap content (1.5%w). As shown in Fig. 1a, mixing Lap and PEO in moderate concentrations led to the formation of a weak shake-gel (type 2). Increasing the clay concentration boosted the mechanical strength to the extent that the gel could sustain its own weight. Motivated by the different physical appearance of the samples, we quantified their viscoelasticity through oscillatory shear. In Fig. 2b, the upward shift in storage and loss moduli by two orders of magnitude clearly evidenced the enhanced mechanical strength of the gel due to the addition of extra clay. Akin to the weak shake-gel, the stiffening

displayed a rapid initial rise and slowed down with the approach of depletion of the Lap from the bulk.

In Fig. 3a, we performed creep experiments on a weak shake-gel (type 2). By following the response of the gel to a step stress, we first observed significant deformation at ca. 3.5 Pa, until at 8.0 Pa the gel deformed plastically. Past that point the sample was unable to recover, indicating that it lost irreversibly any memory of its initial state and was hence no longer fitting the description of a gel. In contrast to the softer gel formed at lower Lap concentrations, the strong shake-gel (type 3) did not plastically deform on applying shear stress as high as 200 Pa, with a final deformation of only about 1.5% (Fig. 3b).

Expanding the analysis of the creep step-stress experiments in Fig. 3, Fig. 4 shows a direct comparison between the strengths of the two shake-gels (types 2 and 3). Specifically, we followed the instantaneous deformation $\delta\gamma_1$, i.e. the strain difference before and after stress application. This allowed us to isolate the net effect of straining the gel solely due to the newly applied stress, eliminating to some extent the dependence on strain history. In this way, we enabled direct comparison between the compliances of the two types of gels. Applying linear regression to the $\delta\gamma_1$ data and comparing the slopes revealed 500-fold enhancement in mechanical strength of the strong shake-gel compared to the weak shake-gel, where the latter displayed an average strain deformation of 2.4% per unit applied stress in a regime well below the yield stress.

Moreover, the instantaneous recovery $\delta\gamma_2$, *i.e.* the strain difference before and after the stress was removed, informed on the gel 'memory' of its previous state. By normalising with respect to the last measured point of applied stress, it was possible to isolate the extent of gel recovery for every step-stress applied. For the weak shake-gel (type 2), $\delta\gamma_2$ steadily decreased with the increase in applied stress, signifying the reduced ability of the gel to recover with the approach of the yield stress. Interestingly, the opposite behaviour was observed in the case of the strong shake-gel (type 3), which exhibited a certain level of strain-thickening and higher degree of recovery at higher stresses. Moreover, the low measured strains in the stiff gel suggested that the break point was much higher than 200 Pa, showing great promise for applications in storage and scaffolding, with a focus on mechanical rigidity. Further, the mechanical properties of these nanocomposites could be finely tuned by changing the clay content.

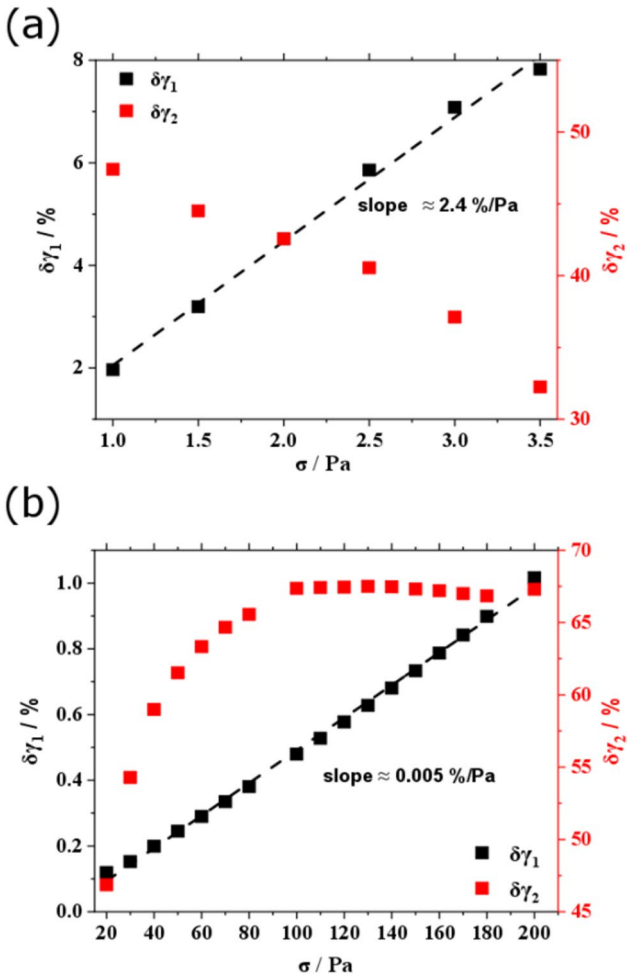

Fig. 4 **a** Creep analysis using data from Fig. 3: plots of instantaneous deformation ($\delta\gamma_1$, black squares) and instantaneous recovery ($\delta\gamma_2$, red squares) on applying shear stress σ. We note that **a** weak gel (type 2) deformed to a much greater extent than **b** strong gel (type 3), with the slope ratio showing roughly 500-fold increase in mechanical strength on increasing the clay content

Bulk rheology on MMT-PEO NCs

To compare with Lap-PEO nanocomposites, we also performed bulk rheology on MMT-PEO suspensions. In Fig. 5, the MMT-PEO mixtures contained fixed concentration of MMT (0.83%w) and three different concentrations of PEO (0.017%w, 0.17%w and 0.85%w). Qualitative inspection of the samples showed the type I mixture with the lowest concentration of PEO to flow readily. The bulk rheology measurements for this sample contained a significant amount of noise due to reaching the sensitivity limit of the instrument (minimum torque ≈ 1 nN*m). Further, the type II mixture displayed propensity towards phase-segregating into a gel-like subnatant and water-like supernatant. Bulk rheology on each layer revealed that the supernatant resembled type I liquid (not shown here), while the gel phase displayed considerable G′(ω) and G″(ω). This viscoelasticity was attributed to the formation of a weaker shake-gel compared to Lap-PEO at the same clay and polymer concentrations. The creep measurement on the type II shake-gel was plotted in the inset of Fig. 5. Even at the low shear stress of 0.1 Pa, the mixture

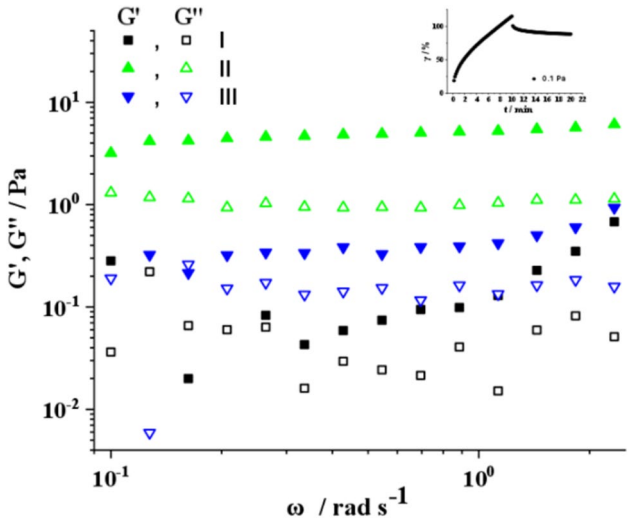

Fig. 5 Frequency ramps displaying the storage (filled symbols) and loss (empty symbols) moduli for each MMT-PEO mixture. Type II shake-gel phase-segregated and measurements on each phase confirmed the presence of a fluid-like supernatant (not shown) and a gel-like subnatant (green triangles). All creep measurements were performed at a fixed strain of 1%. The inset shows the fragile nature of the shake-gel, which deformed by over 100% at 0.1 Pa stress in a creep bulk rheology test

deformed by over 100%, indicating its fragile structure. Finally, type III liquids displayed higher viscosity than type I mixtures owing to the increased PEO concentration. This observation was consistent with the idea that once full coating of the MMT particles was reached, the viscoelastic response was dominated by the excess PEO.

Whereas bulk rheology successfully characterised shake-gels of different mechanics, it displayed low-sensitivity artifacts in measuring more liquid samples. To try and overcome challenges in measuring easily flowing suspensions, we used passive microrheology.

Passive microrheology on Lap-PEO NCs

Here we used DLS-based passive microrheology (Mukhopadhyay et al. 2022) to study the effect of aging on different types of Lap-PEO mixtures prepared without shaking. In Fig. 6, we summarised the electric-field autocorrelation functions $g_1(q, t)$ and MSD results for tracer polystyrene particles dispersed in 0.50%w Lap/0.025%w PEO (type 1, Fig. 6a) and 0.83%w Lap/0.17%w PEO (type 2, Fig. 6b) mixtures. In the type 1 liquid Lap-PEO, we observed little change in viscoelasticity in the first few days, with the sample viscosity only slightly exceeding that of water due to the dispersed polymer and clay. As the sample continued aging (6–9 days waiting time), the correlation decay times in the $g_1(q, t)$ curves progressively increased, indicating a slower relaxation process. The timescale for this process started at a millisecond and increased more than ten-fold over the measured range of waiting times. This was accompanied by shorter lag times to reach sub-diffusive motion of the tracer particles in the MSD plots, corresponding to the stiffening of the Lap-PEO structure.

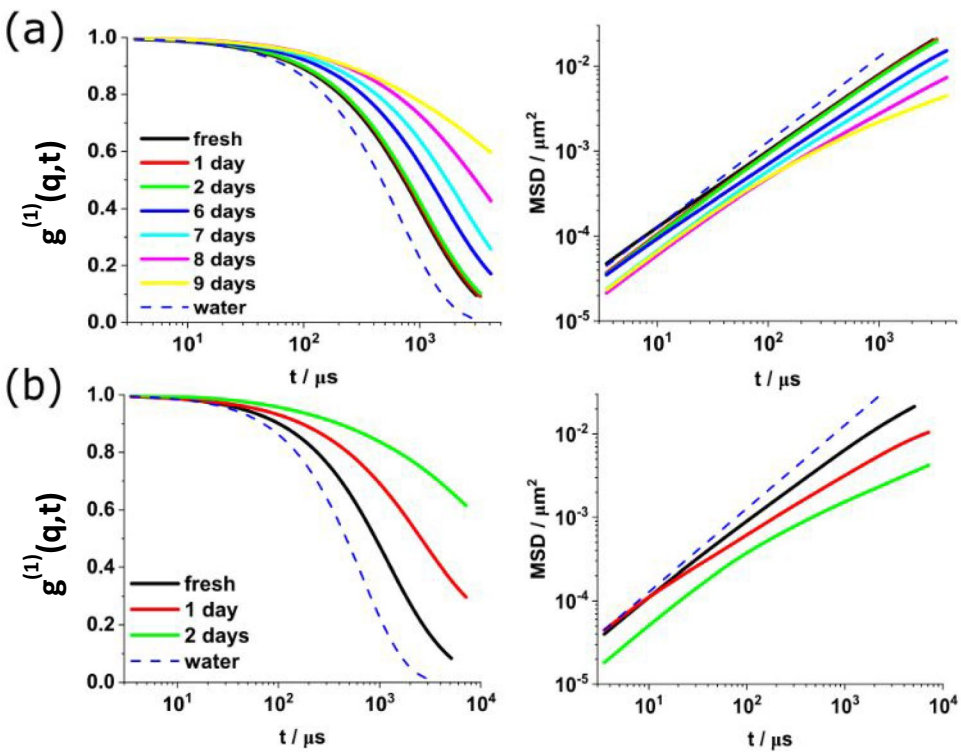

Fig. 6 DLS-based passive microrheology on Lap-PEO mixtures, containing **a** 0.50%w Lap and 0.025%w PEO (type 1 liquid) or **b** 0.83%w Lap and 0.17%w PEO (type 2 weak shake-gel). The intermediate scattering functions in each case show the effect of Lap aging combined with polymer adsorption as the correlation decay time gradually increases. The MSD curves revealed a transition from linear Einstein diffusion to sub-diffusive behaviour, with the onset of sub-diffusion shifting to shorter times with sample aging. Dashed blue curves show the calibration measurements of tracer particles in deionised water, given as reference

A similar trend was present in the type 2 Lap-PEO sample (Fig. 6b), where a much shorter waiting time was required to achieve the same degree of aging as in the type 1 mixture. Even in the absence of shaking, which would otherwise cause the Lap-PEO suspension to form a weak shake-gel, there was a propensity towards gelation, marked by a shift in the correlation decay times and a transition of the MSD to sub-diffusion.

We further compare the aging mechanisms in types 1 and 2 Lap-PEO mixtures in Fig. 7, where we showed viscoelastic data from DLS microrheology. The storage modulus, G′(ω) and the loss modulus, G″(ω) both increased with waiting time, indicating the stiffening of the suspension. However, there was accelerated aging on increasing Lap and PEO concentrations, suggesting that aging is a diffusion-limited process. The cross-over between the two moduli marked the longest relaxation time of the network (30–60 ms). This value was much longer than the 240-μ s decay time in fresh bare Lap suspensions (Zebrowski et al. 2003) and the Zimm relaxation time for 400 kDa PEO of ca. 50 µs (Wu et al. 2019). We attributed this long timescale to the formation of clay aggregates, within which the tracers were confined. These aggregates could be joined by more polymer chains, increasing the number of contact points. Due to the low adsorption energy between Lap and PEO, these contacts continuously broke and reformed subjected to thermal fluctuations. Mode-coupling theory suggested the escape of the probe-particles into the bulk required the collective desorption of many polymer chains from the Lap surface, which could take tens of milliseconds. We observed predominantly viscous behaviour on very short timescales, with the viscosity approaching that of water (blue dashed curves in Fig. 7). On longer timescales, however, the aged samples were mostly elastic, suggestive of the formation of a loose gel structure.

To investigate the effect of shear-thickening, we used passive DWS-based microrheology, where the signal-to-noise was particularly high due to multiple scattering. We compared the viscoelasticity of Lap-PEO nanocomposites before and after shaking (Fig. 8). The decay in the intermediate scattering function (Fig. 8a) reflected the diffusivity of the probe-particles, which indirectly reported on the viscosity of the surrounding medium. We observed very little effect on shaking type 1 Lap-PEO liquids, in which neither the clay content nor the polymer concentration was sufficiently high to cause the formation of a shake-gel. On the other hand, increasing the PEO concentration ten-fold, from 0.017 to 0.17%w (type 1 to type 2) at a fixed concentration of 0.83%w Lap led to a significant rise in viscoelasticity on shaking. The relaxation time quadrupled, shifting from 150 µs to ca. 600 µs. This difference was amplified in the case of the strong shake-gel (type 3), containing 1.50%w Lap. We noted here a deviation from the bulk rheology results. Rich et al. (2011a, b) previously reported rheological inconsistencies between micro- and macroscale with bare Lap suspensions, where analysing the MSD with unconventional methods, such as fractional calculus, might offer an explanation. Here, we conclude that microscopic measurements suggest much

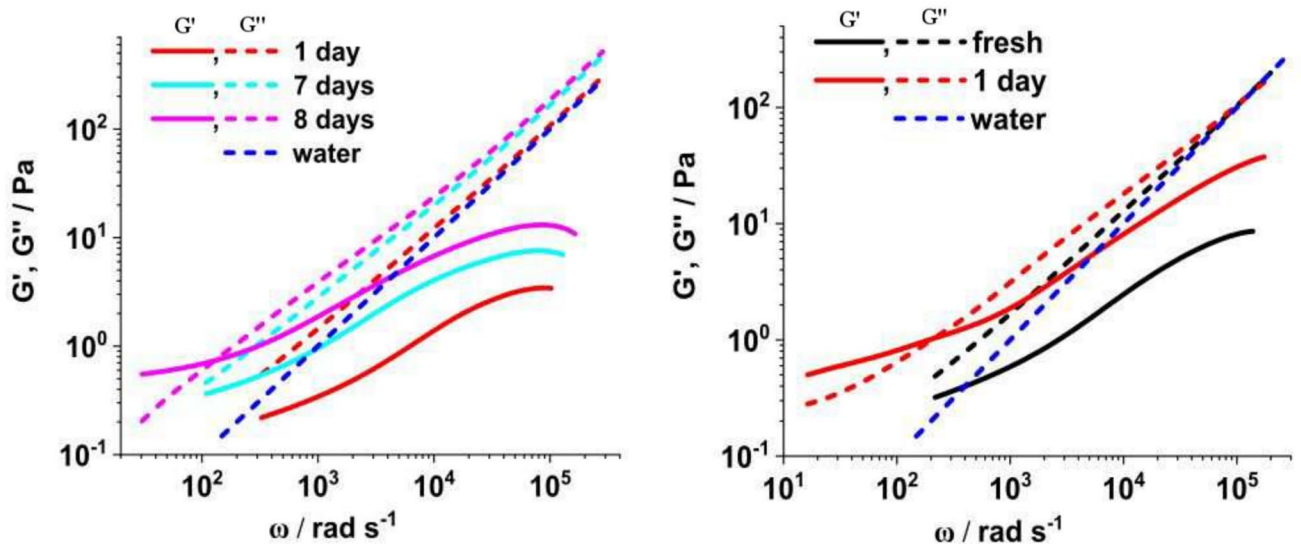

Fig. 7 Storage (G′(ω), solid lines) and loss (G″(ω), dashed lines) moduli from DLS-based microrheology on the Lap-PEO mixtures from Fig. 6. The viscoelasticity of 0.50%w Lap and 0.025%w PEO mixture is shown in the left-hand panel, while the one of 0.83%w Lap and 0.17%w PEO can be seen in the right-hand panel. The upward shift in both moduli clearly indicates the stiffening of the Lap-PEO mixtures, where increasing the Lap and PEO concentrations had the effect of accelerating the aging. Dashed blue line indicates the theoretical loss modulus of deionised water, included as reference

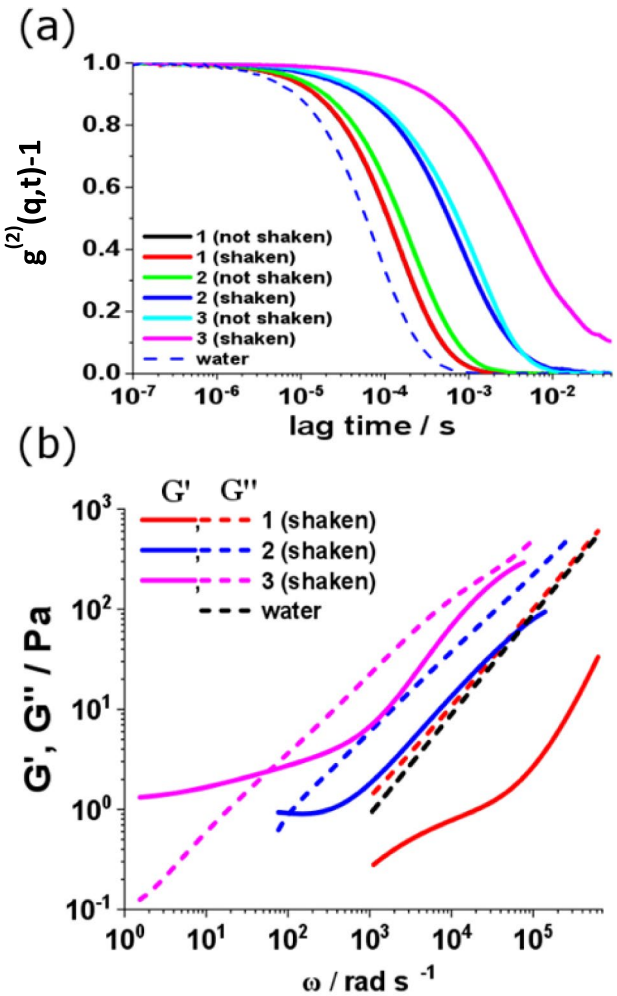

Fig. 8 DWS-based microrheology before and after shaking different types of Lap-PEO mixtures. Type 1 corresponds to a composition of 0.83%w Lap and 0.017%w PEO (liquid); type 2 contains 0.83%w Lap and 0.17%w PEO (weak shake-gel); type 3 has 1.50%w Lap and 0.17%w PEO (strong shake-gel). **a** Intermediate scattering functions for all three mixtures before and after shaking (dashed curve denotes probe-particle calibration in deionised water). **b** Storage (G′(ω), solid lines) and loss (G″(ω), dashed lines) moduli for all three mixtures (dashed black line denotes the loss modulus of water and is included for reference)

weaker gels and longer gelation times than their bulk counterpart (Rich et al. 2011a, b).

In Fig. 8b, we compared the storage and loss moduli of all three types of Lap-PEO mixtures, measured immediately after shaking. In line with the phase diagram and bulk rheology data, the type 1 mixture remained fluid over the probed frequency range. In types 2 and 3, where we expected the formation of weak and strong shake-gels, respectively, we observed the emergence of low-frequency elasticity. The cross-over between G′(ω) and G″(ω) displayed a slight shift to a lower frequency with the increase of Lap content, corresponding to the appearance of a slower relaxation process.

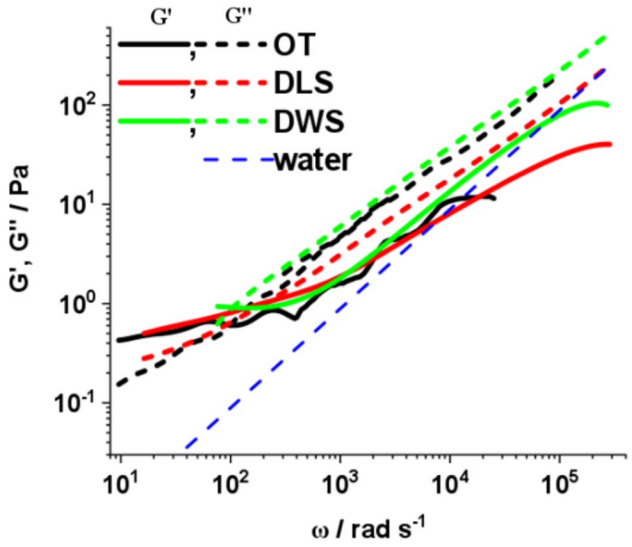

Fig. 9 Comparison between three types of microrheology: single-beam optical tweezers, dynamic light scattering and diffusing wave spectroscopy. All three techniques were performed on the same sample of type 2 Lap-PEO mixture (0.83%w Lap and 0.17% PEO). OT and DLS measurements were performed on a 1-day-old sample (not shaken), while the DWS data collected on a fresh sample (shaken). Storage (G′(ω)) moduli are presented by solid lines, while loss (G″(ω)) moduli are marked by dashed lines. The dashed blue line is included for comparison, denoting the loss modulus of water

In fact, the cross-over frequency for the weak shake-gel was in good agreement with our previous results from DLS, obtained at the exact same clay and polymer concentrations. The longer relaxation time for the strong shake-gel was likely due to Lap clusters now involving a higher number of clay particles compared to type 2 mixtures.

Finally, we showed a comparison of microrheology results on type 2 Lap-PEO (0.83%w Lap and 0.17%w PEO), combining optical tweezers, DLS and DWS into a single plot (cf. Figure 9). We found close agreement among all three techniques. Measuring a 1-day-old sample using OT and DLS yielded very similar G′(ω), while the viscosity given by the high-frequency slope of G″(ω) deviated slightly. This could be attributed to the fact that in single-beam point-trap optical tweezers, the viscoelastic response is highly dependent on the local environment surrounding the probe-particle. On the other hand, ensemble-averaged data from DLS and DWS are less susceptible to local density fluctuations.

The green curves in Fig. 9 represent the final result from DWS-based microrheology on a type 2 Lap-PEO nanocomposite immediately following shaking. Unexpectedly we found good correspondence between an aged sample (1-day-old in this case) and one, which has been subjected to strong shear. Stretching out the polymer through extensional stresses could accelerate the bridging of Lap clusters and therefore cause apparent aging of a fresh sample. The cross-overs observed in the elastic

and viscous moduli were comparable, corresponding to a relaxation time of about 30–60 ms. This value would likely increase with aging, where more Lap from the bulk joins the bridged clusters or the number of Lap-PEO contact points increases.

Employing DLS-based microrheology to study the dynamic mechanical properties of MMT-PEO proved challenging due to the high scattering of the host medium. Therefore, we resorted to measuring the viscoelasticity of these suspensions using DWS alone, where the high scattering from the tracers dominated the signal. The compositions we chose in this study were type I, containing 0.83%w MMT and 0.017%w PEO, and type III, composed of 0.83%w MMT and 0.85%w PEO. The phase-segregating type II mixture was excluded from this study due to (1) the sample's inability to comply with the condition for a system in equilibrium, and (2) the preferential diffusion of the tracers into the clay-poor phase driven by an increase in entropy.

Passive microrheology on MMT-PEO NCs

In Fig. 10, we showed intermediate scattering functions and viscoelastic moduli of two MMT-PEO mixtures. While there was a very small effect of shaking the type I mixture, in which the polymer concentration was insufficient for connecting MMT particles together, there was a noticeable shift in the decay time for the type III mixture (Fig. 10a). The higher initial viscosity of unperturbed type III mixture compared to type I was confirmed by the difference in decay times. The shift observed on shaking the type III mixture was attributed to the formation of larger clay clusters, facilitated by incomplete PEO coverage of the MMT particles. Owing to their larger size compared to Lap, the MMT clay surfaces required more polymer strands for complete steric stabilisation against electrostatic aggregation. The sample remained a fluid on the macroscale, implying that PEO still dominated the dynamics on shearing the nanocomposite.

In Fig. 10b, we showed the storage and loss moduli obtained from converting the intermediate scattering functions from Fig. 10a. The cross-over between G′(ω) and G″(ω) revealed a relaxation time of around 60 ms, as in the case of using Lap-PEO nanocomposites. This observation alone points towards similar adsorption mechanisms driving the assembly of PEO with either Lap or MMT. The size and charge differences between the two types of clay however led to very different phase diagrams when combined with PEO, as already shown in Fig. 1. Further experiments building on this work would involve measuring the viscoelasticity of a percolating shake-gel formed at high MMT concentrations, if challenges related to extracting noise-free data from highly scattering dense samples are first overcome.

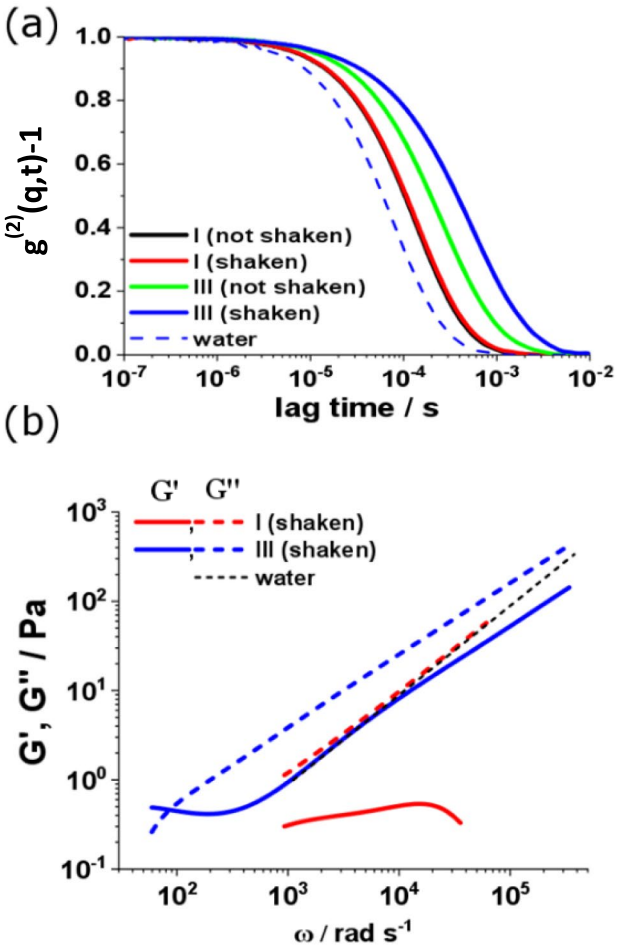

Fig. 10 DWS-based microrheology before and after shaking two different types of MMT-PEO mixtures. Type I corresponds to a composition of 0.83%w MMT and 0.017%w PEO (low-viscosity liquid), while type III contains 0.83%w MMT and 0.85%w PEO (high-viscosity liquid). **a** Intermediate scattering functions for the two mixtures before and after shaking (dashed curve denotes probe-particle calibration in deionised water). **b** Storage (G′(ω), solid lines) and loss (G″(ω), dashed lines) moduli for the two shaken mixtures (dashed black line denotes the loss modulus of water and is included for comparison)

Conclusions

Clay-polymer systems present rich phase diagrams that can be controlled by fine tuning of the concentrations of the building blocks. Rheological measurements on micro- and macroscale offer different routes to testing the mechanical strength and stress rigidity of these clay-polymer phases. Here we showed via oscillatory shear and creep bulk measurements how the stiffness of a Lap-PEO shake-gel could be significantly enhanced by small variations in the clay content. In stark contrast, MMT-PEO mixtures were characterised by a very different phase behaviour, offering a useful comparison between nanocomposites formed by

natural and synthetic clays. DLS and DWS microrheology assays confirmed the physical picture of reversible PEO adsorption and desorption onto the surface of clay particles and provided quantitative information about the viscoelasticity and relaxation times of the mixtures. We expect that these findings will find practical use in the design of biological fluids and pharmaceuticals as well as facilitate the development of new alternatives for long-term storage and flame-retardation gel coatings.

Supplementary Information The online version contains supplementary material available at https://doi.org/10.1007/s00397-025-01499-7.

Acknowledgements We would like to acknowledge Dr. Alessio Caciagli, Dr. Bruno Matarese and Dr. Simon Butler for their help in the setup operation and analysis of our DLS and DWS microrheology data.

Funding Open Access funding enabled and organized by Projekt DEAL. IDS acknowledges financial help from EPSRC (grant no. 1805384). AM acknowledges Commonwealth Scholarship Commission (UK government). RT and EE are supported by the Research Council of Norway through its Centres of Excellence funding scheme (project no. 262644, PoreLab). RT is additionally funded by the Sustainable Stable Ground Project (grant no. 324486). EE further acknowledges the Winton Program for Sustainable Physics in funding this project.

Data Availability Data are available from the corresponding authors upon reasonable request.

Declarations

Conflict of interest The authors declare no competing interests.

References

Baghdadi HA, Jensen EC, Easwar N, Bhatia SR (2008a) Evidence for re-entrant behavior in Laponite–PEO systems. Rheol Acta 47(2):121–127

Baghdadi HA, Parrella J, Bhatia SR (2008b) Long-term aging effects on the rheology of neat Laponite and Laponite–PEO dispersions. Rheol Acta 47:349–357

Baghdadi HA, Sardinha H, Bhatia SR (2005) Rheology and gelation kinetics in Laponite dispersions containing poly(ethylene oxide). J Polymer Sci Part B Polymer Phys 43(2):233–240

Bonn D, Coussot P, Huynh HT, Bertrand F, Debregeas G (2002a) Rheology of soft glassy materials. Europhys Lett 59(5):786–792

Bonn D, Kellay H, Tanaka H, Wegdam G, Meunier J (1999a) Laponite: what is the difference between a gel and a glass? Langmuir 15:7534–7536

Bonn D, Tanaka J, Wegdam G, Kellay H, Meunier J (1999b) Aging of a colloidal "Wigner" glass. Europhys Lett 45(1):52–57

Bonn D, Tanase S, Abou B, Tanaka H, Meunier J (2002b) Laponite: aging and shear rejuvenation of a colloidal glass. Phys Rev Lett 89(1):015701

Brostow W, Dutta M, de Souza JR, Rusek P, Medeiros AMM, Ito EN (2010) Nanocomposites of poly(methyl methacrylate) (PMMA) and montmorillonite (MMT) Brazilian clay: a tribological study. Express Polym Lett 4:570–575

Cabane B, Wong K, Lindner P, Lafuma F (1997) Shear induced gelation of colloidal dispersions. J Rheol 41:531–547

Can V, Okay O (2005) Shake gels based on Laponite-PEO mixtures: effect of polymer molecular weight. J Des Mon Polym 8(5):453–462

Evans RML, Tassieri M, Auhl D, Waigh TA (2009) Direct conversion of rheological compliance measurements into storage and loss moduli. Phys Rev E 80:012501

Harden JL, Viasnoff V (2001) Recent advances in DWS-based microrheology. Curr Op in Coll and Int Sci 6(5–6):438–445

Ho DL, Briber RM, Glinka CJ (2001) Characterization of organically modified clays using scattering and microscopy techniques. Chem Mater 13:1923–1931

Jin YH, Park HJ, Im SS (2002) Polyethylene/clay nanocomposite by in-situ exfoliation of montmorillonite during Ziegler-Natta polymerization of ethylene. Macromol Rapid Commun 23:135–140

Langmuir I (1938) The role of attractive and repulsive forces in the formation of tactoids, thixotropic gels, protein crystals and coacervates. J Chem Phys 6:873–896

Leach ESH, Hopkinson A, Franklin K, van Duijneveldt JS (2005) Non-aqueous suspensions of Laponite and montmorillonite. Langmuir 21:3821–3830

Lemaire BJ, Panine P, Gabriel JCP, Davidson P (2002) The measurement by SAXS of the nematic order parameter of Laponite gels. Europhys Lett 59:55–61

Levitz P, Lecolier E, Mourchid A, Delville A, Lyonnard S (2000) Liquid–solid transition of Laponite suspensions at very low ionic strength: long-range electrostatic stabilisation of anisotropic colloids. Europhys Lett 49:672–677

Li L, Harnau L, Rosenfeldt S, Ballauff M (2005) Effective interaction of charged platelets in aqueous solution: investigations of colloid Laponite suspensions by static light scattering and small-angle x-ray scattering. Phys Rev E 72:051504

Maier T, Boehm H, Haraszti T (2012) Splinelike interpolation in particle tracking microrheology. Phys Rev E 86:011501

Mason TG (2000) Estimating the viscoelastic moduli of complex fluids using the generalized Stokes-Einstein equation. Rheol Acta 39:371–378

Mason TG, Weitz DA (1995) Optical measurements of frequency-dependent linear viscoelastic moduli of complex fluids. Phys Rev Lett 74(7):1250–1253

Morariu S, Bercea MJ (2009) Effect of addition of polymer on the rheology and electrokinetic features of Laponite RD aqueous dispersions. Chem Eng Data 54:54–59

Mourchid A, Delville A, Lambard J, Lecolier E, Levitz P (1995) Phase-diagram of colloidal dispersions of anisotropic charged particles-equilibrium properties, structure, and rheology of Laponite suspensions. Langmuir 11(6):1942–1950

Mourchid A, Lecolier E, Van Damme H, Levitz P (1998) On viscoelastic, birefringent, and swelling properties of Laponite clay suspensions: revisited phase diagram. Langmuir 14(17):4718–4723

Mourchid A, Levitz P (1998) Long-term gelation of Laponite aqueous dispersions. Phys Rev E 57(5):R4887–R4890

Mukhopadhyay A, Stoev ID, King DA, Sharma KP, Eiser E (2022) Amyloid-like aggregation in native protein and its suppression in the bio-conjugated counterpart. Front Phys 10:535–547

Murray HH (2000) Traditional and new applications for kaolin, smectite, and palygorskite: a general overview. Appl Clay Sci 17(5–6):207–221

Pignon F, Magnin A, Piau JM, Cabane B, Lindner P, Diat O (1997) Yield stress thixotropic clay suspension: investigations of structure by light, neutron, and x-ray scattering. Phys Rev E 56:3281–3289

Provencher SW (1982) A constrained regularisation method for inverting data represented by linear algebraic or integral equations. Comp Phys Comm 27:213–227

Raji M, Mekhzoum MEM, el Qaiss AK, Bouhfid R (2016) Nanoclay reinforced polymer composites: nanocomposites and bionanocomposites. Springer 1:1–34

Ramsay JDFJ (1986) Colloidal properties of synthetic hectorite clay dispersions. Colloid Interface Sci 109:441–447

Rich JP, Lammerding J, McKinley GH, Doyle PS (2011a) Nonlinear microrheology of an aging, yield stress fluid using magnetic tweezers. Soft Matter 7:9933–9943

Rich JP, McKinley GH, Doyle PS (2011b) Size dependence of microprobe dynamics during gelation of a discotic colloidal clay. J Rheol 55:273–299

Ruzicka B, Zaccarelli E (2011) A fresh look at the Laponite phase diagram. Soft Matter 7:1268–1286

Schmidt G, Nakatani AI, Butler PD, Karim A, Han CC (2000) Shear orientation of viscoelastic polymer-clay solutions probed by flow birefringence and SANS. Macromolecules 33(20):7219–7222

Schmidt G, Nakatani AI, Han CC (2002) Rheology and flow birefringence from viscoelastic polymer-clay solutions. Rheol Acta 41(1–2):45–54

Stoev ID, Caciagli A, Xing Z, Eiser E (2018) Using single-beam optical tweezers for the passive microrheology of complex fluids. Proc SPIE 10723:107232D

Tyan HL, Wu CY, Wei KH (2001) Effect of montmorillonite on thermal and moisture absorption properties of polyimide of different chemical structures. J Appl Polym Sci 81:1742–1747

van Olphen H (1977) An introduction to clay colloid chemistry: for clay technologists, geologists, and soil scientists. Science 143:1023–1024

Weitz DA, Zhu JX, Durian DJ, Gang H, Pine DJ (1993) Diffusing-wave spectroscopy: the technique and some applications. Phys Scr T49:610–621

Wu X, Zhao Z, Kang Y, Ji X, Liu Y (2019) Viscoelasticity of poly(ethylene glycol) in aqueous solutions of potassium sulfate: a comparison of quartz crystal microbalance with conventional methods. Polym J 51:471–480

Xu P, Lan Y, Xing Z, Eiser E (2018) Liquid crystalline behaviour of self-assembled LAPONITE/PLL-PEG nanocomposites. Soft Matter 14:2782–2788

Zebrowski J, Prasad V, Zhang W, Walker LM, Weitz DA (2003) Shake-gels: shear-induced gelation of Laponite–PEO mixtures. Colloids Surf A Physicochem Eng Asp 213(2–3):189–197